1-1-2006

Power System Control with an Embedded Neural Network in Hybrid System Modeling

Seung-Mook Baek

Jung-Wook Park

Ganesh K. Venayagamoorthy
Missouri University of Science and Technology

Recommended Citation

S. Baek et al., "Power System Control with an Embedded Neural Network in Hybrid System Modeling," *Conference Record of the 41st IAS Annual Meeting of the Industry Applications Conference, 2006*, Institute of Electrical and Electronics Engineers (IEEE), Jan 2006.
The definitive version is available at https://doi.org/10.1109/IAS.2006.256595

Power System Control with an Embedded Neural Network in Hybrid System Modeling

Seung-Mook Baek and Jung-Wook Park
Power IT and System Laboratory
School of Electrical and Electronic Engineering
YONSEI University
134 Sinchon-dong, Seodaemun-gu, Seoul, Korea
jungpark@yonsei.ac.kr

Ganesh K. Venayagamoorthy
Real-Time Power and Intelligent Systems Laboratory
Dept. of Electrical and Computer Engineering
University of Missouri-Rolla
132 Emerson Electric Co. Hall, MO, 65409-0249, USA
ganeshv@ece.umr.edu

Abstract— **The output limits of the power system stabilizer (PSS) can improve the system damping performance immediately following a large disturbance. Due to non-smooth nonlinearities from the saturation limits, these values cannot be determined by the conventional tuning methods based on linear analysis. Only *ad hoc* tuning procedures can been used. A feedforward neural network (FFNN) (with a structure of multilayer perceptron neural network) is applied to identify the dynamics of an objective function formed by the states, and thereafter to compute the gradients required in the nonlinear parameter optimization. Moreover, its derivative information is used to replace that obtained from the trajectory sensitivities based on the hybrid system model with the differential-algebraic-impulsive-switched (DAIS) structure. The optimal output limits of the PSS tuned by the proposed method are evaluated by time-domain simulation in both a single machine infinite bus system (SMIB) and a multi-machine power system (MMPS).**

Keywords-component; **Feedforward neural network, hybrid system, nonlinearities, non-smoothness, parameter optimization, power system stabilizer.**

I. INTRODUCTION

The hybrid systems have recently attracted considerable attentions to carry out research in many physical systems, which exhibit a mix of continuous dynamics, discrete-time and discrete-event dynamics, switching action, and jump phenomena [1], [2]. For typical disturbances, the power system stabilizer (PSS) used to damp system low-frequency oscillations is an important control objective in the hybrid system application because the non-smooth nonlinear dynamic behavior due to a saturation limiter falls into a category of the hybrid systems in that an event occurs when a controller signal saturates.

The dynamic behavior of the PSS is affected by the linear parameters (gain and time constants of phase compensator) and the constrained parameters (saturation output limits) resulting in non-smooth nonlinear behavior. The proper selection of linear parameters has been usually made based on conventional tuning techniques [3]-[6] using the small signal stability analysis. However, by focusing only on small signal conditions, the dynamic damping performance immediately following a *large disturbance* is often degraded. The PSS output limits (which cannot be determined by the linear approach) can provide the solution to balance theses competing effects. In particular, these limit values attempt to prevent the machine terminal voltage from falling below the exciter reference level while speed is also falling, which means that it can improve the reduced transient recovery after disturbance (faster recovery to its initial steady state points, therefore, it allows to save system energy), especially in multi-machine power systems.

In this study, the hybrid systems applied to the parameter optimization for the PSS output limits are modeled by a set of *differential-algebraic-impulsive-switched* (DAIS) structure reported in [7], where the derivative information of a model was obtained by the computation of the trajectory sensitivities through the exact modeling of a plant. However, in some practical applications, the exact modeling for a physical nonlinear device (for example, a switching device such as a pulse-width-modulated inverter) may not be accomplished. Also, the calculation of derivatives of a complex system (such as a large-scale power system) requires the highly computational efforts. The artificial neural network (ANN) can be an alternative to replace the computation of the first-order derivatives from the trajectory sensitivities in the DAIS structure for the hybrid system model. Because the ANN is able to adaptively model or identify a nonlinear multiple-input multiple-output (MIMO) plant without requiring the exact mathematical modeling of plant [8].

This paper makes the new contribution by applying a feedforward neural network (FFNN) to the hybrid system modeling to compute the first-order derivatives required for the nonlinear parameter optimization of the PSS in power systems. The performance of the PSS nonlinear controller tuned optimally by the proposed method is assessed by the case

This work was supported by the Yonsei University, Seoul, Korea under Grant No. 2005-1-0333 and the National Science Foundation, USA under the CAREER Grant: ECS # 0348221.

studies carried out on a single machine infinite bus system (SMIB) and a multi-machine power system (MMPS).

II. Hybrid System Presentation

As already mentioned, hybrid systems, which include power systems, are characterized by the following:

- Continuous and discrete states.
- Continuous dynamics.
- Discrete events or triggers.
- Mappings that define the evolution of discrete states at events.

In other words, the hybrid system is a mathematical model of physical process consisting of an interacting continuous and discrete event system. A formal presentation of the hybrid system is given in [9], where a general hybrid dynamical system is defined as $H = [Q, \sum, A, G]$ and

- Q is the set of discrete states;
- $\sum = \{\sum_q\}_{q\in Q}$ is the collection of dynamical systems $\sum_q = [X_q, \Gamma_q, f_q]$ where each X_q is an arbitrary topological space forming the continuous state space of $\sum_q$, Γ_q is a semigroup over which the states evolve, and f_q generates the continuous state dynamics;
- $A = \{A_q\}_{q\in Q}$, $A_q \subset X_q$ for each $q \in Q$, is the collection of autonomous jump sets, i.e., the conditions which trigger jumps;
- $G = \{G_q\}_{q\in Q}$, where G_q: $A_q \rightarrow S = U_{q\in Q}(X_q \times \{q\})$ is the autonomous jump transition map. The hybrid state-space of H is given by S.

The above level of abstraction of the general hybrid system does not suit the implementation of numerical optimization method carried out in this study, for which the first-order derivative information can be exploited efficiently. A hybrid model with the DAIS structure, which is more conducive to such analysis, can be presented without loss of generalities as follows [7].

$$\dot{\underline{x}} = \underline{f}(\underline{x}, y) \tag{1}$$

$$0 = g(\underline{x}, y) \tag{2}$$

$$0 = \begin{cases} g^{(i-)}(\underline{x}, y) & y_{d,i} < 0, \\ g^{(i+)}(\underline{x}, y) & y_{d,i} > 0, \end{cases} \quad i = 1, \cdots, d \tag{3}$$

$$\underline{x}^{+} = \underline{h}_j(\underline{x}^{-}, y^{-}) \quad y_{e,j} = 0, \quad j \in \{1, \cdots, e\} \tag{4}$$

where

$$\underline{x} = \begin{bmatrix} x \\ z \\ \lambda \end{bmatrix}, \quad \underline{f} = \begin{bmatrix} f \\ 0 \\ 0 \end{bmatrix}, \quad \underline{h}_j = \begin{bmatrix} x \\ h_j \\ \lambda \end{bmatrix},$$

$$\underline{x} \in X \subseteq \Re^{\underline{n}}, \; y \in Y \subseteq \Re^m, \; z \in Z \subseteq \Re^l, \; \lambda \in L \subseteq \Re^p,$$

and

- x are the continuous dynamic states, for example generator angles, speed, and fluxes.
- z are discrete dynamic states, such as transformer tap positions and protection relay logic states.
- y are algebraic states, e.g. load bus voltage magnitudes and angles.
- λ are parameters such as generator reactance, controller gains, switching times, and limit values.

The differential equations $\underline{f}$ in (1) are correspondingly structured for $\dot{x} = \underline{f}(\underline{x}, y)$, whilst z and λ remain constant away from events. Similarly, the reset equations $\underline{h}_j$ in (4) ensure that x and λ remain constant at reset events, but the dynamics states z are reset to new values according to $z^{+} = h_j(\underline{x}^{-}, y^{-})$ (The notation $\underline{x}^{+}$ denotes the value of $\underline{x}$ just after the reset event, while $\underline{x}^{-}$ and y^{-} refer the values of $\underline{x}$ and y just prior to the event). The algebraic function g in (2) is composed of $g^{(0)}$ together with appropriate choices of $g^{(i-)}$ or $g^{(i+)}$, depending on the signs of the corresponding elements of y_d in (3). An event is triggered by an element of y_d changing sign and/or an element of y_e in (4) passing through zero. In other words, at an event, the composition of g changes and/or elements of z are reset.

Then, the system flows ϕ are defined accordingly as

$$\phi(\underline{x}_0, t) = \begin{bmatrix} \phi_{\underline{x}}(\underline{x}_0, t) \\ \phi_y(\underline{x}_0, t) \end{bmatrix} = \begin{bmatrix} \underline{x}(t) \\ y(t) \end{bmatrix}. \tag{5}$$

The full detailed explanation and associated mathematical equations of the DAIS model (especially for the *switching and impulse effects*) are given in [7] with the comprehensive studies of the hybrid system.

III. Nonlinear Controller Optimization

In engineering multivariable nonlinear problems, numerical optimization methods play the significant part to find the solutions of nonlinear functions on complex systems or select the parameters by which the objective function **J** can be minimized or maximized. The optimal tuning problem for the PSS output limits described in this paper is the case of the latter. Again, in this study the gradient information required for the nonlinear parameter optimization is obtained by the FFNN applied to the hybrid system, instead of the computation of the trajectories sensitivities through the exact modeling of a plant.

A. *Implementation of Optimal Tuning Applied to PSS*

A single machine infinite bus system (SMIB) is shown in Fig. 1. The PSS and the automatic voltage regulator (AVR) controllers in Fig. 2 are connected to the generator (**G**) of the SMIB system. The generator (**G**) is accurately represented by a

six-order machine model, viz., a two axis (*d-q*) model with two damper windings in each axis [10].

The output (clipping) limits on the PSS output V_{PSS} and the anti-windup limits on the field voltage E_{fd} in Fig. 2 introduce events that can be captured by the DAIS model. In other words, the event occurs when a controller signal saturates in the response to the large inputs ($\Delta\omega$ and V_t) due to the disturbance. This indicated phenomenon is implemented by the DIAS structure as given in (6) and (7) for the PSS clipping limits and AVR anti-windup limits, respectively.

$$\begin{aligned} &y_1 = \mathrm{V}_{\max} - \mathrm{V}_{\text{out}}; \\ &y_2 = \mathrm{V}_{\text{out}} - \mathrm{V}_{\min}; \\ 0 = &\begin{cases} g_1^{(i-)}(\underline{x},y) = \mathrm{V}_{\text{PSS}} - \mathrm{V}_{\max} & y_1 < 0, \\ g_1^{(i-)}(\underline{x},y) = \mathrm{V}_{\text{PSS}} - \mathrm{V}_{\min} & y_2 < 0, \\ g_1^{(i+)}(\underline{x},y) = g_2^{(i+)}(\underline{x},y) = \mathrm{V}_{\text{PSS}} - \mathrm{V}_{\text{out}} & y_1 > 0, y_2 > 0. \end{cases} \end{aligned} \tag{6}$$

$$\begin{aligned} &y_3 = \mathrm{E}_{\text{fdmax}} - E_{fd}; \quad y_4(\text{upper limits switch}) : (+ \text{ when } y_3 < 0) \\ &y_5 = E_{fd} - \mathrm{E}_{\text{fdmin}}; \quad y_6(\text{lower limits switch}) : (+ \text{ when } y_5 < 0) \\ 0 = &\begin{cases} g_3^{(i-)}(\underline{x},y) = y_4 - 1 & y_3 < 0, \\ g_4^{(i-)}(\underline{x},y) = E_{fd} - \mathrm{E}_{\text{fdmax}} & y_3 < 0, \\ g_5^{(i-)}(\underline{x},y) = y_6 - 1 & y_5 < 0, \\ g_6^{(i-)}(\underline{x},y) = E_{fd} - \mathrm{E}_{\text{fdmin}} & y_5 < 0, \\ g_3^{(i+)}(\underline{x},y) = g_5^{(i+)}(\underline{x},y) = y_4 = y_6 & y_3 > 0, y_5 > 0, \\ g_4^{(i+)}(\underline{x},y) = g_6^{(i+)}(\underline{x},y) = \mathrm{K}_{\text{A}} \cdot x_{trg} - E_{fd} & y_3 > 0, y_5 > 0. \end{cases} \end{aligned} \tag{7}$$

Many practical optimization problems can be formulated using a Bolza form of the objective function **J**

$$\min_{\lambda, t_f} \mathbf{J}(\underline{x}, y, \lambda, t_f) \tag{8}$$

$$\text{suject to} \begin{bmatrix} \underline{x}(t) \\ y(t) \end{bmatrix} = \phi(\underline{x}_0, t), \text{ where } \underline{x} \in S \text{ (constraint set)} \tag{9}$$

$$\mathbf{J} = \varphi\left(\underline{x}(t_f), y(t_f), \lambda, t_f\right) + \int_{t_0}^{t_f} \psi\left(\underline{x}(t), y(t), \lambda, t\right) dt, \tag{10}$$

where λ are the optimized parameters (output limits in this study) that are adjusted to minimize the value of objective function **J** in (10), and t_f is the final time. The objective of tuning the PSS controller is to mitigate system damping and force the system to recover to the post-disturbance stable operating point as quickly as possible. The speed deviation ($\Delta\omega$) and terminal voltage deviation (ΔV_t) of the generator in Fig. 2 are considered as good assessments of the damping and recovery [6]. Therefore, the objective function **J** in (10) can be re-formulated for the optimal tuning of the PSS with specific time t_f as the following

$$\mathbf{J}(\lambda) = \int_{t_0}^{t_f} \left(\begin{bmatrix} \omega(\lambda,t) - \omega^s \\ V_t(\lambda,t) - V_t^s \end{bmatrix}^T \mathbf{V} \begin{bmatrix} \omega(\lambda,t) - \omega^s \\ V_t(\lambda,t) - V_t^s \end{bmatrix} \right) dt, \tag{11}$$

where **V** is the weighting matrix. The ω^s and V_t^s are the post-fault steady state values of ω and V_t, respectively. Note that the diagonal terms in the matrix **V** are determined by considering the balance of the conflicting requirements on the speed and voltage deviations.

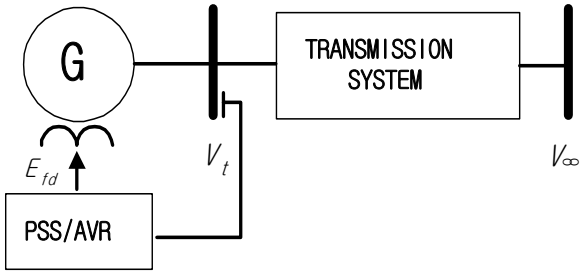

Fig. 1. Single machine infinite bus system (SMIB).

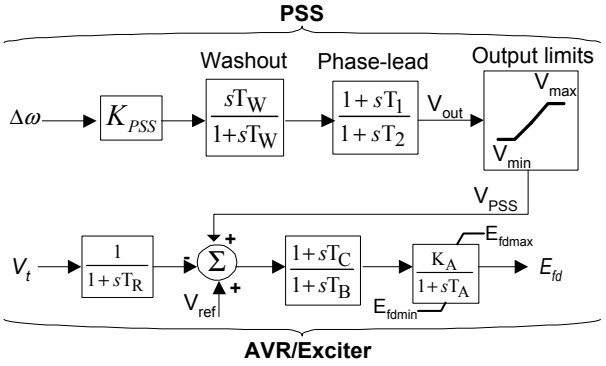

Fig. 2. AVR/PSS block representation.

B. *Computation of Gradient by the FFNN*

To minimize the value of the function $\mathbf{J}(\lambda)$ in (10), the first-order derivatives of **J** with respect to λ (V_{max} and V_{min}) need to be estimated by the FFNN shown in Fig. 3. This FFNN (with the multilayer perceptron structure) consists of three-layers of neurons (which are the input, hidden, and output layer in Fig. 4) interconnected by the weight matrices $\mathbf{W}_I$ and $\mathbf{W}_L$, and it is first designed to identify the dynamics of the plant.

The activation function for neurons in the hidden layer in Fig. 4 is given by the following sigmoidal function.

$$s(x) = \frac{1}{1+\exp(-x)} \tag{12}$$

The output layer neurons are formed by the inner products between the nonlinear regression vector from the hidden layer and the output weight matrix. Generally, the FFNN starts with random initial values for its weights, and then computes a one-pass backpropagation algorithm [11] at each time step k, which consists of a forward pass propagating the input vector through the network layer by layer, and a backward pass to update the weights with the error signal between $\mathbf{J}$ and $\tilde{\mathbf{J}}$ shown in Fig. 3.

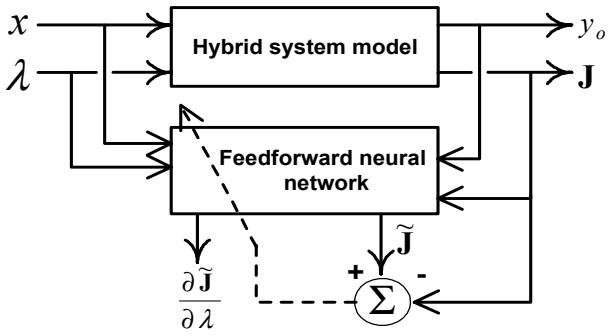

Fig. 3. Feedforward neural network applied to the hybrid system.

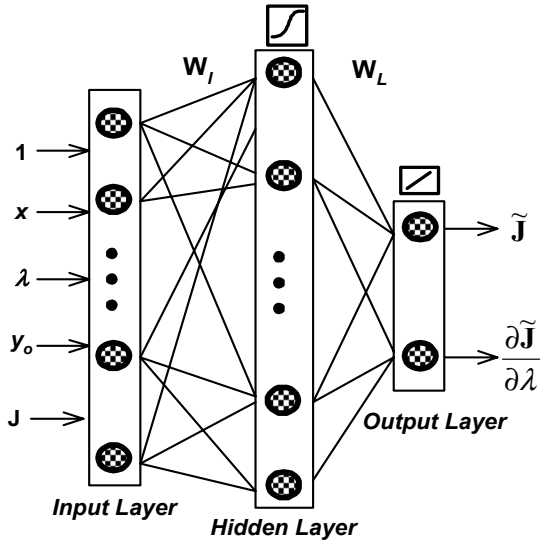

Fig. 4. Structure of the FFNN.

The functional expression ζ of the FFNN used for this study is given as

$$\left(\tilde{\mathbf{J}}(k), \frac{\partial \tilde{\mathbf{J}}}{\partial \lambda}(k)\right) = \zeta\left(x(k-1), y_o(k-1), \lambda(k-1), \mathbf{J}(k-1)\right) \quad (13)$$

where k denotes the time index and

- $x = [\Delta\omega, \Delta V_t]$.
- $y_o = V_{PSS}$ (in Fig. 2).
- $\lambda = [V_{max}\ V_{min}]$ (in Fig. 2).
- $\mathbf{J}$ is the output of the objective function defined in (11).

After training the weights of the FFNN for 100 s (in simulation time) in off-line, the identification performance of the function $\mathbf{J}$ by the FFNN is evaluated, and the result is shown in Fig. 5, where the values of $\mathbf{J}$ are the corresponding responses when a large-disturbance (a 100 ms three-phase short circuit) is applied to the generator terminal bus in Fig. 2 at t = 0.05 s. And, the final time t_f in (11) is 5 s. It is obvious from the result that the FFNN is able to identify the objective function $\mathbf{J}$ with sufficient accuracy.

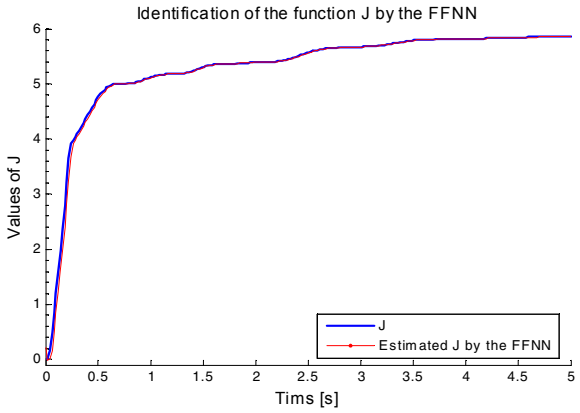

Fig. 5. Identification of the function $\mathbf{J}$ by the FFNN.

Thereafter, the gradient $\nabla\tilde{\mathbf{J}}(\lambda) = \partial\tilde{\mathbf{J}}/\partial\lambda$ is calculated by the back-stepping computation based on the chain-rule through the FFNN [11], and it is given as

$$\begin{aligned}\nabla\tilde{\mathbf{J}}(\lambda) &= \frac{\partial\tilde{\mathbf{J}}}{\partial\lambda} = \frac{\partial\tilde{\mathbf{J}}}{\partial t}\frac{\partial t}{\partial p_L}\frac{\partial p_L}{\partial q_L}\frac{\partial q_L}{\partial p_l}\frac{\partial p_l}{\partial q_l}\frac{\partial q_l}{\partial\lambda} \\ &= \left\{s(q_l)\left(1-s(q_l)\right)\mathbf{W}_l(\lambda)\right\}\sum_{j=1}^{m_l}\tilde{\mathbf{J}}\cdot\mathbf{W}_L\end{aligned} \quad (14)$$

where:

- t is target value.
- m_l is the number of neurons in the hidden layer.
- p is the output of the activation function for a neuron.
- q *is* the regression vector as the activity of a neuron.
- $\mathbf{W}$ is the weight matrix.
- L and l denote the output and hidden layer, respectively.
- The function s is the sigmoidal function in (12).

The variations of $\nabla\tilde{\mathbf{J}}(\lambda) = \partial\tilde{\mathbf{J}}/\partial\lambda$ by the FFNN at each iteration are shown in Figs. 6 and 7, respectively. Then, these nonlinear parameters λ are updated by using (15) with $\nabla\tilde{\mathbf{J}}(\lambda)$ during iteration. It is clearly shown from Figs. 6 and 7 that the absolute values of gradients are decreased after each iteration and converged to their optimal local minimum in the *sub-*

optimal space formed when applying the large-disturbance (three-phase short circuit) to the plant.

$$\lambda_{k+1} = \lambda_k + \alpha \cdot \nabla \tilde{\mathbf{J}}(\lambda) \tag{15}$$

where α is the step–length.

At the end of each run, the convergence performance is evaluated by the user-defined criterion, which are the maximum relative changes in parameters (S_C) as given in (16) as well as the value of **J**. Note that the parameter optimization problem by the FFNN aims to minimize the value of objective function $\mathbf{J}(\lambda)$ with the small number of iterations.

$$S_C = \left\| \frac{\lambda_{k+1} - \lambda_k}{\lambda_{k+1}} \right\|_\infty . \tag{16}$$

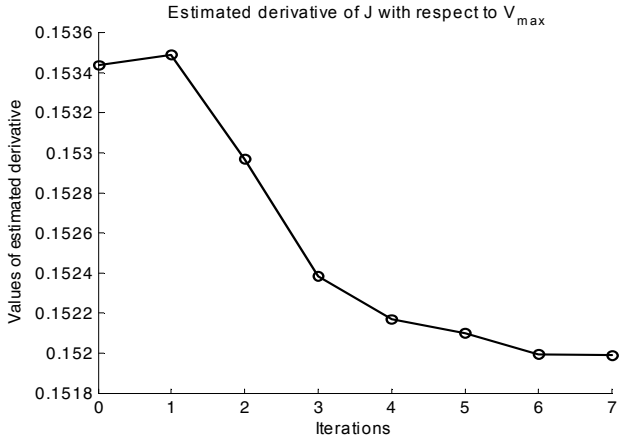

Fig. 6. The values of $\partial\tilde{\mathbf{J}} / \partial V_{max}$ by the FFNN at each iteration.

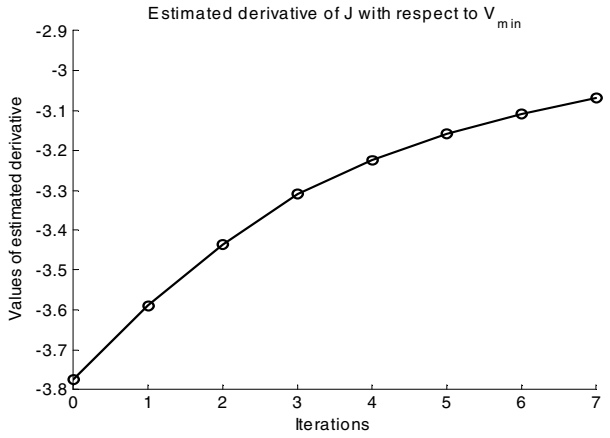

Fig. 7. The values of $\partial\tilde{\mathbf{J}} / \partial V_{min}$ by the FFNN at each iteration.

IV. Case Studies

A. *Test in Single Machine Infinite Bus System*

During the optimization process (iteration) applied to the SMIB system in Fig. 1, the values of the objective function **J** variations are shown in Fig. 8. It can be said from this result that the FFNN is successfully applied to the hybrid system model for the PSS output limits, and therefore to minimize the values of **J** in this nonlinear parameter optimization problem. The corresponding maximum relative changes (S_C) in (16) at each iteration are also given in Fig. 9. It might be valuable to compare the convergence speed by any other improved numerical optimization such as the conjugate-gradient or quasi-Newton methods.

The damping performance of the output limits (which are [0.1105 –0.3365] for [V_{max} V_{min}]) of the PSS optimized after 7 iterations is compared with that of the initial output limits ([0.1 –0.1]) by applying the 100 ms three-phase fault at the generator terminal bus in Fig. 1 at 0.05 sec. The simulation results are given in Figs. 10 and 11. It is clearly shown that the optimal saturation limits determined by the proposed method improve the system dynamic damping and transient terminal voltage response effectively. The value of V_{max} has been changed a little from 0.1 to 0.1105, but the value of V_{min} has moved significantly from –0.1 to –0.3365. The effect of optimal tuning for these saturation limits is rather dramatic and quite evident for a large disturbance (such as a three-phase short circuit) applied to a power system. The corresponding PSS output response (V_{PSS}) in Fig. 12 exhibits the non-smooth nonlinear dynamic behaviors. Note that a lowering of V_{min} is quite counter-intuitive; manual tuning would likely not even search in that direction for improved response.

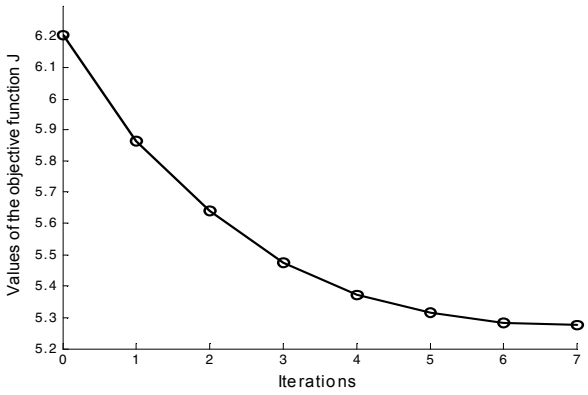

Fig. 8. Values of the objective function **J** variations.

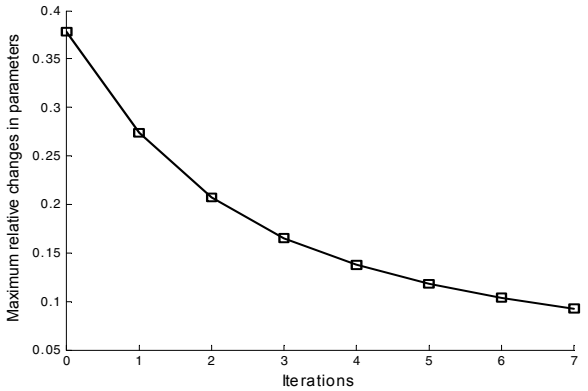

Fig. 9. Maximum relative changes in the optimized parameters.

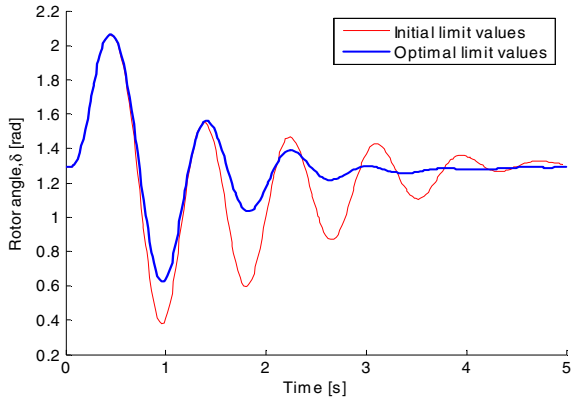

Fig. 10. Generator rotor angle response [rad].

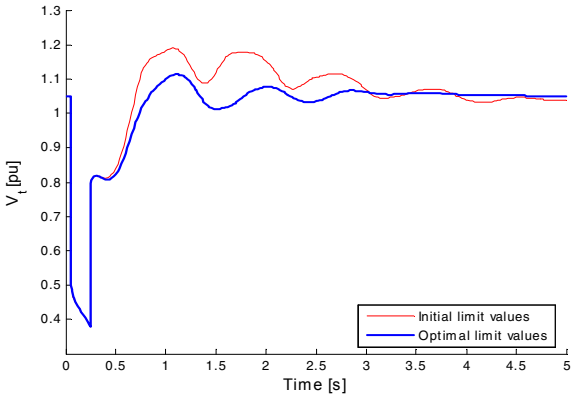

Fig. 11. Generator terminal voltage response [pu].

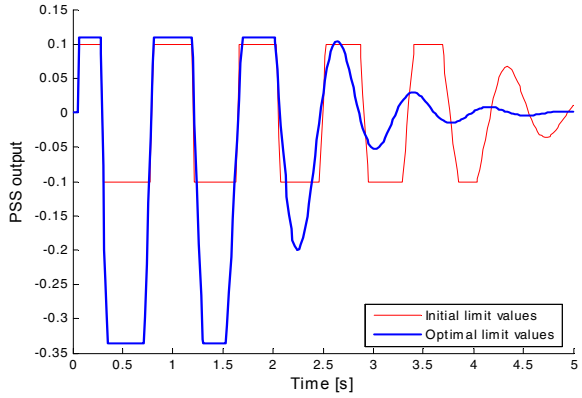

Fig. 12. PSS output response.

B. *Test in Multi-Machine Power System*

The four-machines, two-area test system is shown in Fig. 13. The data of this system is given in [6]. Each machine has been presented by a fourth-order nonlinear model [10]. All generators (G1 to G4) are equipped with the AVR/PSS system shown in Fig. 2.

The effect of the optimal limits values of the multi-PSSs on the MMPS in Fig. 13 with respect to the damping performance is investigated. The objective function **J** in (11) is re-defined for the application to the MMPS as

$$\mathbf{J}(\lambda)=\sum_{i=1}^{4}\int_{t_0}^{t_f}\left(\begin{bmatrix}\omega_i(\lambda,t)-\omega_i^s\\ V_{t,i}(\lambda,t)-V_{t,i}^s\end{bmatrix}^T\mathbf{V}\begin{bmatrix}\omega_i(\lambda,t)-\omega_i^s\\ V_{t,i}(\lambda,t)-V_{t,i}^s\end{bmatrix}\right)dt, \quad (17)$$

where the subscript i is the generator number in Fig. 13.

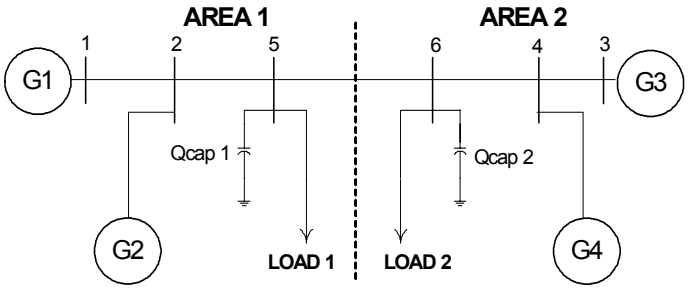

Fig. 13. Four-machine two-area test system.

While minimizing the single value of the **J** in (17), the proposed method is applied to determine the optimal output limits of the local PSSs, which are affected by the interactions of each other on the multi-machine power network. This application gives a good example for the *global dynamic optimization* of large-scale complex systems.

The total 21 inputs and 36 neurons are used in the input and hidden layers of the FFNN, respectively. As the procedure described in Section III, after training the weights of the FFNN in off-line, the parameters λ (output limits of all PSSs) are updated by (15) with the gradients $\nabla\tilde{\mathbf{J}}(\lambda)=\partial\tilde{\mathbf{J}}/\partial\lambda$ computed through the FFNN by (14) during the optimization process.

It is clearly shown from Fig. 14 that the values of the objective function **J**, which are corresponding to the updated parameters, are minimized at each iteration. After 10 iterations in Fig. 14, the values of the optimized output limits are given in Table I with those of the initial output limits.

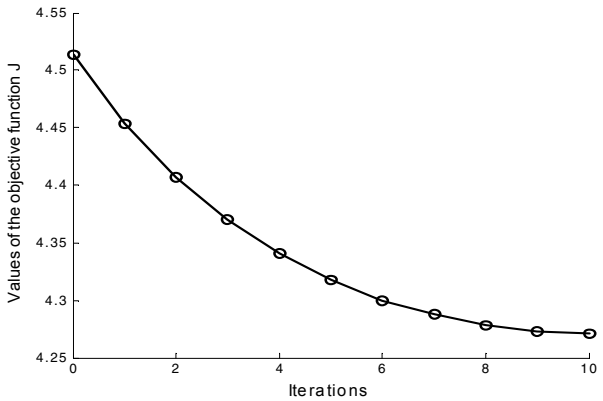

Fig. 14. Values of the objective function **J** variations: test on the MMPS.

TABLE I
INITIAL VS. OPTIMAL LIMIT VALUES OF PSSS

Output limits	Initial [V_{max} V_{min}]	Optimal [V_{max} V_{min}]
PSS-G1	[0.05 –0.05]	[0.0992 –0.1268]
PSS-G2	[0.05 –0.05]	[0.1021 –0.0828]
PSS-G3	[0.1 –0.1]	[0.1533 –0.2558]
PSS-G4	[0.1 –0.1]	[0.1484 –0.1938]

The damping performance by the PSSs with the optimized output limits is evaluated by applying the 150 ms three-phase fault at bus 5 in Fig. 13 at 0.1 s. The relative speed oscillations ($\Delta\omega_1$-$\Delta\omega_2$ and $\Delta\omega_3$-$\Delta\omega_4$) for the deviation signals in AREA 1 and 2 are given in Figs. 15 to 16, respectively. Also, the relative speed oscillation ($\Delta\omega_1$-$\Delta\omega_3$) between AREA 1 and 2 is shown in Fig. 17. The simulation results show that the dynamic performance to damp out the low-frequency oscillations is effectively improved by the optimized output limits, which are non-smooth nonlinear parameters. Especially, the damping in AREA 2 is remarkably improved compared to that in AREA 1. Correspondingly, the parameter variations in AREA 2 are higher than those in AREA 1 (see Table I).

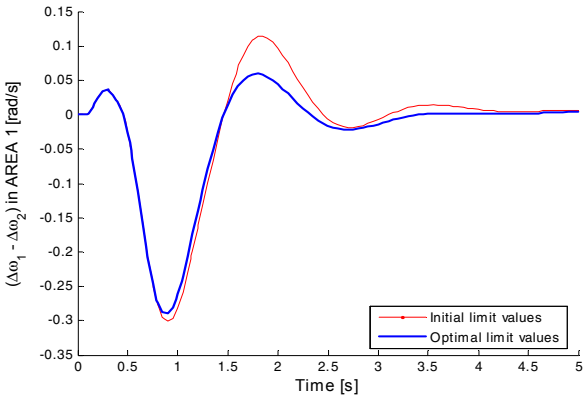

Fig. 15. Relative speed oscillations ($\Delta\omega_1$-$\Delta\omega_2$) in AREA 1 [rad/s].

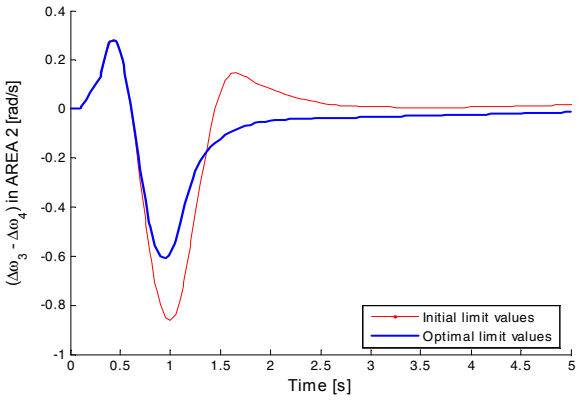

Fig. 16. Relative speed oscillations ($\Delta\omega_3$-$\Delta\omega_4$) in AREA 2 [rad/s].

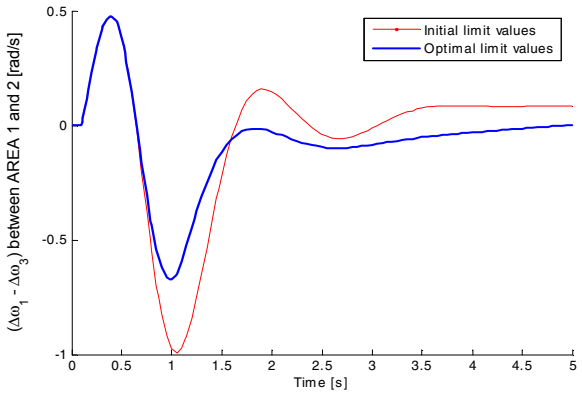

Fig. 17. Relative speed oscillations ($\Delta\omega_1$-$\Delta\omega_3$) between AREA 1 and 2 [rad/s].

V. CONCLUSIONS

In this paper, the output limits of the power system stabilizer (PSS) in a power system were considered as the parameters to be optimized by using the hybrid system model with the differential-algebraic-impulsive-switched (DAIS) structure. To implement the nonlinear parameter optimization, the feedforward neural network (FFNN) was applied to this hybrid system model to compute the gradients of the objective function **J** with respect to the PSS output limits. In other words, the FFNN was used as an alternative to replace the computation of the first-order derivatives from the trajectory sensitivities. Therefore, this paper made the new contribution by applying the hybrid system, which combines analytical modeling with the soft-computing method such as an artificial neural network, to the power system control.

The availability of the FFNN in the hybrid system modeling makes it possible to avoid the exact modeling of the overall plant, and thereby to reduce the computational efforts required in a large-scale complex hybrid system. It is still an open question as to which gradient-based method is the most appropriate. Steepest descent method by the gradients computed through the FFNN may require many iterations with low convergence speed. This situation can be avoided by the conjugate-gradient and quasi-Newton type methods, which provide an estimate of second derivatives.

ACKNOWLEDGMENT

The authors would like to thank Prof. Ian A. Hiskens in the Department of Electrical and Computer Engineering, University of Wisconsin-Madison, USA for his original contributions on the hybrid systems modeling with the differential-algebraic-impulsive-switched (DAIS) structure and the useful suggestions therein, which also had an influence on this paper.

REFERENCES

[1] A. van der Schaft and H. Schumacher, An Introduction to Hybrid Dynamical Systems, Springer-Verlag, London, 2000.

[2] D. Liberzon, Switching in Systems and Control, Birkhauser, Boston, 2003.

[3] P. Kundur, M. Klein, G.J. Rogers, and M.S. Zywno, "Application of Power System Stabilizers for Enhancement of Overall System Stability," *IEEE Trans. on Power Systems*, Vol.4, No.2, pp. 614-626, May 1989.

[4] M. Klein, G. J. Rogers, S. Moorty, and P. Kundur, "Analytical Investigation of Factors Influencing Power System Stabilizers Performance", *IEEE Trans. on Energy Conversion,* Vol. 7, No. 3, pp. 382-388, September 1992.

[5] N. Martins and L. T. G. Lima, "Determination of Suitable Locations for Power System Stabilizers and Static VAr Compensators for Damping Electromechanical Oscillations in Large Scale Power Systems", *in Proc. of Power Industry Computer Application*, pp.74-82, May 1989.

[6] Prabha Kundur, "Power system stability and Control," EPRI Editors, McGraw-Hill, Inc. 1993, ISBN 0-07-035958-X.

[7] Ian A. Hiskens and M. A. Pai, "Trajectory Sensitivity Analysis of Hybrid Systems", *IEEE Trans. on Circuits and Systems-Part I: Fundamental Theory and Applications*, Vol.47, No.2, pp. 204-220, February 2000.

[8] K. Narendra, and K. Parthasarathy, "Identification and Control of Dynamical Systems Using Neural Networks," *IEEE Trans. on Neural Networks*, Vol.1, No.1, pp. 4-27, March 1990.

[9] M. S. Branicky, V. S. Borkar, and S. K. Mitter, " A unified framework for hybrid control: Model and optimal control theory", *IEEE Trans. on Automat. Contr.,* Vol. 43, pp. 31-45, January 1998.

[10] P. W. Sauer and M. A. Pai, *Power System Dynamics and Stability*. Englewood Cliffs, NJ: Prentice-Hall, 1998.

[11] Jung-Wook Park, G.K. Venayagamoorthy, and R.G. Harley, "MLP/RBF Neural-Networks-Based Online Global Model Identification of Synchronous Generator", *IEEE Transactions on Industrial Electronics*, Vol.52, No. 6. pp. 1685-1695, December 2005.